An active fault tolerant control approach to an offshore wind turbine model

Fengming Shi and Ron Patton

School of Engineering

University of Hull

HU6 7RX, Hull, UK

Abstract: The paper proposes an observer based active fault tolerant control (AFTC) approach to a non-linear large rotor wind turbine benchmark model. A sensor fault hiding and actuator fault compensation strategy is adopted in the design. The adapted observer based AFTC system retains the well-accepted industrial controller as the baseline controller, while an extended state observer (ESO) is designed to provide estimates of system states and fault signals within a linear parameter varying (LPV) descriptor system context using linear matrix inequality (LMI). In the design, pole-placement is used as a time-domain performance specification while H_∞ optimization is used to improve the closed-loop system robustness to exogenous disturbances or modeling uncertainty. Simulation results show that the proposed scheme can easily be viewed as an extension of currently used control technology, with the AFTC proving clear "added value" as a fault tolerant system, to enhance the sustainability of the wind turbine in the offshore environment.

Key words: Wind turbine control; Active fault tolerant control; Fault estimation; Linear parameter varying system; Closed-loop robustness; Linear matrix inequalities; Descriptor systems

1 Introduction

As an economically, socially as well as ecologically sustainable renewable energy, wind energy [1] is attracting more and more attention along with the increasing awareness of the need to protect the global environment and in view of the depletion of fossil resources. As a result, wind turbines are contributing more and more to energy production [2] as shown in Fig 1, along with the increasing size of the standard wind turbine systems.

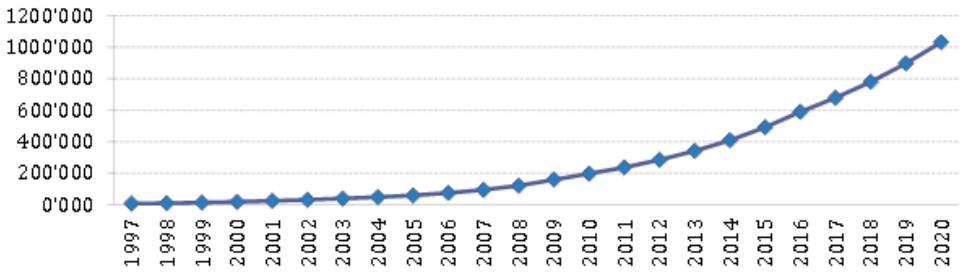

Fig 1 Total installed capacity of wind turbine during 1997-2020 [MW] [2]

Large rotor wind turbines installed recently are expensive and far from living zones, often offshore escalating the requirements of safety, reliability and maintainability [3-7]. An attractive candidate solution is to introduce fault detection and isolation (FDI) and fault tolerant control (FTC) techniques since the control system play an important role in the operation of the wind turbine [8-10] and different control strategies may be considered for different wind turbines systems. In the light of these developments there have been two benchmark models presented in [11, 12] to design robust fault detection and FTC systems for modern large rotor wind turbines; Based on the two models, many results have been presented [13]such as the results presented in [14-17]. The fault tolerant control strategy in [14] considers the low wind speed region using a T-S fuzzy modelling approach while the approach in [15] considers the high speed wind region using a geometric approach. A fault detection and isolation system for rotor current

sensors in a doubly-fed induction generator for wind turbine applications is presented in [16] based on the generalized observer scheme. However, none of these studies consider the robustness of the closed-loop system. On the other hand, in [17] the closed-loop robustness is studied, albeit only for the low wind speed region, considering sensor fault tolerance.

Linear parameter varying (LPV) descriptor systems [18, 19] can provide good design freedom to achieve desired system robustness, closed-loop stability and performance. The power of this approach stems from the combined use of differential and algebraic equations in descriptor systems and the potential to account for rational system parameter variations when using LPV modelling and feedback for estimation or control. In particular, extended state observer (ESO) of LPV descriptor systems approaches can facilitate the estimation of system states and sensor and actuator faults [20, 21].

This paper develops the descriptor system active fault tolerant control (AFTC) scheme within an LPV framework as developed in [20] with application to the wind turbine benchmark proposed in [12] which is naturally nonlinear. The remainder of the paper is organized as follows: The system model with the baseline controller in high wind speed region is depicted in Section 2. Since it is common to demand to retain the practically proved baseline controller when a more advance control scheme is employed, an observer based active fault tolerant control system is designed in Section 3. An integrated AFTC scheme is described using an ESO which provides estimates of both system states and faults. Section 4 shows the simulation results for different faults, including sensor faults, and actuator faults. Conclusions are given in Section 5.

2 Wind turbine system description

A typical wind turbine can be depicted as in Fig 2. The goal of this study is to develop an AFTC control scheme of a benchmark wind turbine model described by [12]. The purpose of the benchmark is to compare and evaluate FDI and fault accommodation designs, as well as FTC schemes with view to selecting the most promising approaches for real wind turbine system applications. The benchmark model is of a three blade horizontal wind turbine which consists of static aerodynamic, drive train, generator, converter and pitch systems. The wind turbine benchmark system has several faults which effectively act in different subsystems.

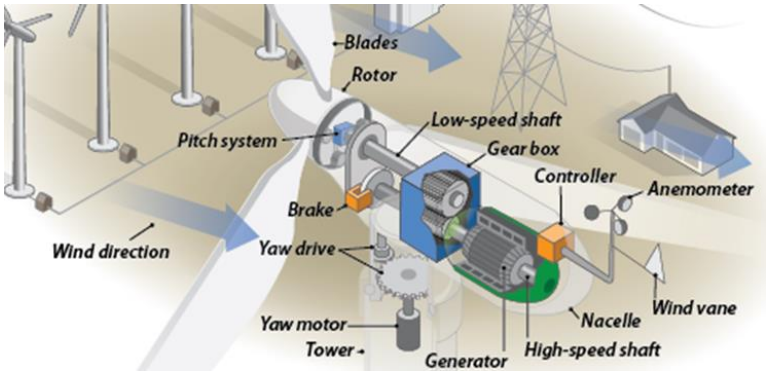

Fig 2 A typical wind turbine structure [22]

2.1 Aerodynamics

The aerodynamics of the wind turbine are modelled terms of the aerodynamic torque $T_r(t)$ acting on the rotor blades, represented by:

$$T_r(t) = \sum_{i=1}^{3} \frac{\rho \pi R^3 C_q(\lambda(t), \beta_i(t)) v_\omega^2(t)}{6} \quad (1)$$

where C_q is the torque coefficient table described by Fig 3, $\beta_i(t)$ is the pitch angle for the i^{th} rotor blade, where $i = 1,2,3$. ρ is the air density; R is the radius of the area swept by the blades; $v_\omega(t)$ is the effective wind speed. This model is valid for small

differences between the $\beta_i(t)$ values. When $\beta_1(t)$, $\beta_2(t)$ and $\beta_3(t)$ are equal, $T_r(t)$ is then rewritten as:

$$T_r(t) = \frac{1}{2}\rho\pi R^3 C_q(\lambda,\beta)v_\omega^2 = KC_q(\lambda,\beta)v_\omega^2 \quad (2)$$

Another important parameter is the power coefficient table $C_p(\lambda,\beta)$, which has a relationship with $C_q(\lambda,\beta)$ [5] as:

$$C_p(\lambda,\beta) = \lambda C_q(\lambda,\beta) \quad (3)$$

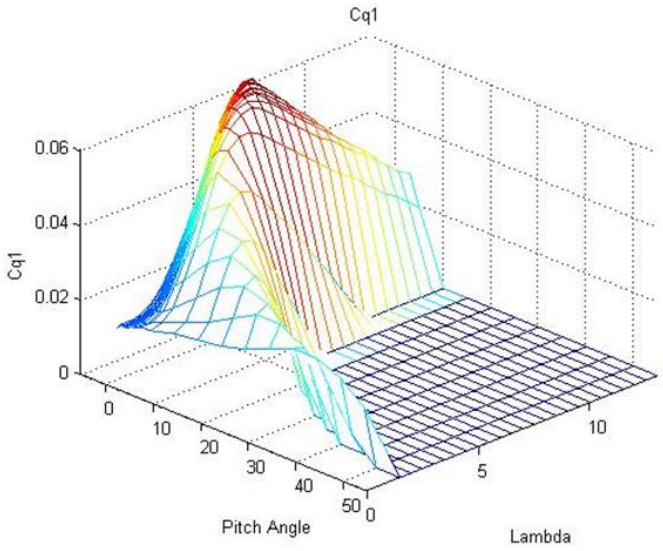

Fig 3 Rotor aerodynamic torque coefficient table

2.2 Drive train

The drive train is described as the following linear system:

$$\begin{bmatrix}\dot{\omega}_r(t)\\ \dot{\omega}_g(t)\\ \dot{\theta}_\Delta(t)\end{bmatrix} = \begin{bmatrix}-\frac{B_{dt}+B_r}{J_r} & \frac{B_{dt}}{N_g J_r} & \frac{-K_{dt}}{J_r}\\ \frac{\eta_{dt}B_{dt}}{N_g J_g} & \frac{-\frac{\eta_{dt}B_{dt}}{N_g^2}-B_g}{J_g} & \frac{\eta_{dt}K_{dt}}{N_g J_g}\\ 1 & -\frac{1}{N_g} & 0\end{bmatrix}\begin{bmatrix}\omega_r(t)\\ \omega_g(t)\\ \theta_\Delta(t)\end{bmatrix} + \begin{bmatrix}\frac{1}{J_r} & 0\\ 0 & -\frac{1}{J_g}\\ 0 & 0\end{bmatrix}\begin{bmatrix}T_r(t)\\ T_g(t)\end{bmatrix} \quad (4)$$

where is J_r the moment of inertia of the low speed shaft, K_{dt} is the torsion stiffness of the drive train, B_{dt} is the torsion damping coefficient of the drive train, B_g is the

viscous friction of the high speed shaft, N_g is the gear ratio, J_g is the moment of inertia of the high speed shaft, η_{dt} is the efficiency of the drive train, and $\theta_\Delta(t)$ is the torsion angle of the drive train. The potential faults in this subsystem include faults acting in the generator and turbine rotor speeds.

2.3 Generator and convertor systems

The converter dynamics can be modelled by a first order transfer function.

$$\frac{T_g(s)}{T_{g,r}(s)} = \frac{\alpha_{gc}}{s+\alpha_{gc}} \tag{5}$$

where α_{gc} is the time parameter of the generator subsystem. The power produced by the generator is given by:

$$P_g(t) = \eta_g \omega_g(t) T_g(t) \tag{6}$$

The potential fault in this subsystem is an offset actuator fault.

2.4 Pitch system

The hydraulic pitch system is modelled as a closed-loop transfer function. In principle these are position servo systems which can be modelled quite well by a second order transfer function [12] as follows:

$$\frac{\beta(s)}{\beta_r(s)} = \frac{\omega_n^2}{s^2+2\cdot\varsigma\omega_n\cdot s+\omega_n^2} \tag{7}$$

where ω_n and ς are the frequency and damping ration parameters, respectively. A drop of oil pressure will change the dynamics of the pitch systems. The pressure level is modelled as a convex combination of the vertices of the two parameters ω_n^2 and $\varsigma\omega_n$. Hence the pitch system can be described in terms of the so-called fault effectiveness parameter $\theta_f(t) \in [0 \quad 1]$, where as $\theta_f(t) = 0$ corresponds to a fault-free actuator

with $\omega_n^2 = \omega_{n0}^2, \varsigma\omega_n = \varsigma_0\omega_{n0}$, $\theta_f(t) = 1$ corresponds to a full fault on the actuator with $\omega_n^2 = \omega_{nf}^2, \varsigma\omega_n = \varsigma_f\omega_{nf}$. Hence, the parameters ω_n^2 and $\varsigma\omega_n$ can be described in terms of the pitch actuator fault, as:

$$\omega_n^2 = \left(1 - \theta_f(t)\right)\omega_{n0}^2 + \theta_f(t)\omega_{nf}^2 \tag{8}$$

$$\varsigma\omega_n = \left(1 - \theta_f(t)\right)\varsigma_0\omega_{n0} + \theta_f(t)\varsigma_f\omega_{nf} \tag{9}$$

From a mathematical standpoint there are no unique state space realizations for a given input-output transfer function. In the original model, the pitch system is obtained by [Apb,Bpb,Cpb,Dpb]=tf2ss([omega_n^2],[1 2*xi*omega_n omega_n^2]). Using the above Matlab command, the obtained state space model will be:

$$\begin{bmatrix}\ddot{\beta}_x \\ \dot{\beta}_x\end{bmatrix} = \begin{bmatrix}-2\varsigma\omega_n & -\omega_n^2 \\ 1 & 0\end{bmatrix}\begin{bmatrix}\dot{\beta}_x \\ \beta_x\end{bmatrix} + \begin{bmatrix}1 \\ 0\end{bmatrix}\beta_r$$

$$y = [0 \quad \omega_n^2]\begin{bmatrix}\dot{\beta}_x \\ \beta_x\end{bmatrix}$$

where β_x is a system variable and the output y is the pitch angle. One problem of the above realization is that the occurrence of an actuator fault (for instance, from $\omega_n^2 = \omega_{n0}^2, \varsigma\omega_n = \varsigma_0\omega_{n0}$, $\theta_f(t) = 1$ to $\omega_n^2 = \omega_{nf}^2, \varsigma\omega_n = \varsigma_f\omega_{nf}$) will lead to a peak in the output which is far from realistic. Hence, it is important here to use a state variable system as follows:

$$\begin{bmatrix}\dot{\beta} \\ \ddot{\beta}\end{bmatrix} = \begin{bmatrix}0 & 1 \\ -\omega_n^2 & -2\varsigma\omega_n\end{bmatrix}\begin{bmatrix}\beta \\ \dot{\beta}\end{bmatrix} + \begin{bmatrix}0 \\ \omega_n^2\end{bmatrix}\beta_r \tag{10}$$

$$y = [1 \quad 0]\begin{bmatrix}\beta \\ \dot{\beta}\end{bmatrix} \tag{11}$$

The realization of (10) and (11) is also used in the work [19]. We can see that the system states will be continuous and not change suddenly in the presence of changes of system dynamics. Furthermore, the pitch system (10) and (11) is equivalent to:

$$\begin{bmatrix}\dot{\beta}\\ \ddot{\beta}\end{bmatrix}=\begin{bmatrix}0 & 1\\ -\omega_{n0}^2 & -2\varsigma_0\omega_{n0}\end{bmatrix}\begin{bmatrix}\beta\\ \dot{\beta}\end{bmatrix}+\begin{bmatrix}0\\ \omega_{n0}^2\end{bmatrix}\beta_r+F_\beta f_\beta \tag{12}$$

$$f_\beta=\begin{bmatrix}\omega_{nf}^2-\omega_{n0}^2 & 2\varsigma_f\omega_{nf}-2\varsigma_0\omega_{n0}\end{bmatrix}x_\beta\theta_f+(\omega_{nf}^2-\omega_{n0}^2)\beta_r\theta_f, F_\beta=\begin{bmatrix}0\\1\end{bmatrix}$$

Remark 1: One benefit of the above transformation is to simplify the design of the observer based AFTC system. However, the potential problem is that the new signal $f_\beta$may not be able to reflect well enough the severity of the original fault θ_f. One way to recover the original fault signal is to use:

$$\theta_f=\frac{f_\beta}{\begin{bmatrix}\omega_{nf}^2-\omega_{n0}^2 & 2\varsigma_f\omega_{nf}-2\varsigma_0\omega_{n0}\end{bmatrix}x_\beta+(\omega_{nf}^2-\omega_{n0}^2)\beta_r}$$

if $\begin{bmatrix}\omega_{nf}^2-\omega_{n0}^2 & 2\varsigma_f\omega_{nf}-2\varsigma_0\omega_{n0}\end{bmatrix}x_\beta+(\omega_{nf}^2-\omega_{n0}^2)\beta_r\neq 0$. To improve the original fault estimation accuracy, one can calculate the estimated fault over a time window of length t_Δ instead of each sampling time. In this way, the error introduced by the disturbance or noise will be reduced effectively. Moreover, the introduction of this time window can avoid singularity in the fault calculation.

2.5 Baseline control in full load operation

As discussed in [12], medium and large-scale wind turbines, which are variable speed and variable pitch wind turbines, are generally designed to work in two regions – the low wind speed region (sometimes known as the partial load region) and the high wind speed region (sometimes known as the full load region). The control objective is to catch as much energy as possible in the partial load region, while the objective in the

full load region is to reduce loads by producing a rated power output at a constant rotor speed.

For the high wind speed zone, the desired operation of the wind turbine is to keep the rotor speed and the generator power at constant values. The main idea is to use the pitch system to control the efficiency of the aerodynamics while applying the rated generator torque. However, in order to improve tracking of the power reference and cancel steady state errors on the output power, a power controller is usually considered as well [3, 8, 9]. Hence, both speed control and power control are included in practice.

The speed controller is implemented as a proportional integral (PI) controller that is able to track the speed reference and cancel possible steady-state errors on the generator speed. The linear speed controller usually has the PI transfer function:

$$D_s(s) = K_{ps}\left(1 + \frac{1}{T_{is}s}\right) \tag{13}$$

where K_{ps} is the proportional gain and $T_{is}$is the integral gain.

The power controller is implemented in order to cancel possible steady state errors on the output power. The power controller is realized as a PI controller in the form:

$$D_p(s) = K_{pp}\left(1 + \frac{1}{T_{ip}s}\right) \tag{14}$$

where K_{pp} is the proportional gain and T_{ip} is the integral rate.

3 Observer-based AFTC design

The baseline controller scheme is already known to work well for real systems and has been proved by a huge number of installed wind turbine systems in healthy conditions [3]. Therefore, it is reasonable to require that the baseline controller is retained in an

AFTC system that has an additional control function used to compensate for the effects of possible faults. In the absence of faults the system reverts back to the baseline control action. The AFTC system makes use of the base-line control as the control system that operates in the normal condition, i.e. when it is considered that no faults are acting.

3.1 The structure

In the study, the basic idea is to design observer-based AFTC system considering the existing baseline controller. The structure of the AFTC is shown in Fig 4.

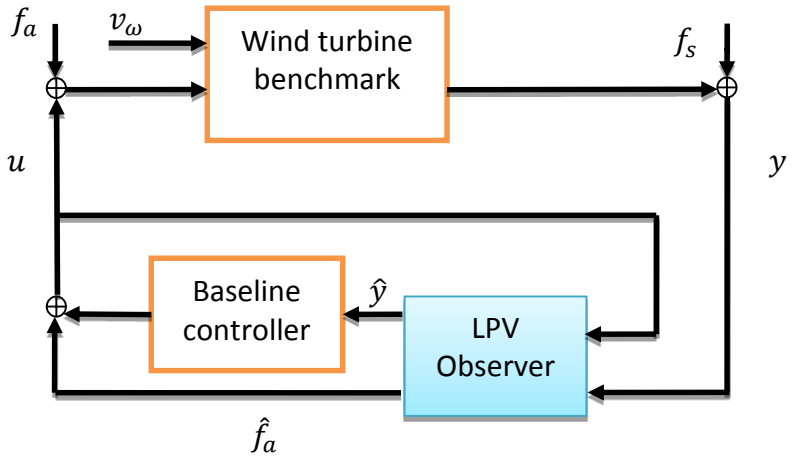

Fig 4 Structure of AFTC with state & faults estimation observer

From this structure and the outline of baseline controller given presented in Section 3, it can be seen that both the actuator fault signals and system outputs should be estimated because of the effects of the sensor faults and sensor noise. In this study, an output feedback FTC scheme is adopted to maintain consistency with the existing practical controller based on the two step design procedure given in Section 4.

The controller used here has an output estimate feedback structure:

$$u_{FTC} = u_{norm} - K_f \hat{f}_a, u_{norm} = K(\theta)\hat{y} \quad (15)$$

where u_{norm} is the baseline controller and $K_f\hat{f}_a$ is used to compensate the effect of actuator faults. In this study, $K(\theta)$ is constant and designed using tradition gain scheduling methods which have been approved widely for real application in wind turbine systems.

3.2 Open-loop LPV system model

For the purpose of design (estimation and control), an LPV model is used obtained by linearizing the non-linear wind turbine system along a suitable operating state trajectory dependent on the wind speed as scheduling parameter. Hence, the modelling uncertainty can be considered to arise mainly from uncertainty in the knowledge of the wind speed, since the effective wind speed in the rotor system is not the same as the anemometer measurement which is assumed in the benchmark.

In the design, the partial derivatives of the nonlinear function for the aerodynamic torque T_r (given by (2)) is evaluated along the desired trajectory in terms of wind speed to obtain total derivative descriptions in terms of $\tilde{T}_r$, $\tilde{v}$, $\tilde{\beta}$, and $\tilde{\omega}_r$ indicating deviations from the design equilibrium point (EQ) values $\bar{T}_r$, $\bar{V}$, $\bar{\beta}$, and $\bar{\omega}_r$, as follows:

$$\tilde{T}_r = \left.\frac{\partial T_r}{\partial v}\right|_{EQ}\tilde{v} + \left.\frac{\partial T_r}{\partial \beta}\right|_{EQ}\tilde{\beta} + \left.\frac{\partial T_r}{\partial \omega_r}\right|_{EQ}\tilde{\omega}_r = T_{r,v}\tilde{v} + T_{r,\beta}\tilde{\beta} + T_{r,\omega_r}\tilde{\omega}_r \tag{16}$$

where:

$$T_{r,\omega_r} = \frac{\bar{T}_r}{\bar{\omega}_r}\left.\frac{\partial C_q/\partial\lambda}{C_q/\lambda}\right|_{EQ}, T_{r,v} = \frac{\bar{T}_r}{\bar{V}}\left(2 - \left.\frac{\partial C_q/\partial\lambda}{C_q/\lambda}\right|_{EQ}\right), T_{r,\beta} = \frac{\bar{T}_r}{\bar{\beta}}\left.\frac{\partial C_q/\partial\beta}{C_q/\beta}\right|_{EQ}$$

In LPV design, the set Θ containing all values of θ on the operating trajectory can be selected to contain the operating locus to a strict region [5]. Furthermore, since the operating locus can be parameterized in terms of the wind speed V [5], so that in this

case the LPV model must also be parameterized in terms of V. Thus, the scheduling parameter can be defined as:

$$\theta = V \tag{17}$$

The partial derivatives are calculated along the normal operating trajectory [5] and shown in Fig 5 together with β, ω_g and λ, where (a), (b) and (c) are for T_{r,ω_r}, $T_{r,\beta}$ and $T_{r,v}$ respectively and (d), (e) and (f) are for β, ω_g and λ respectively.

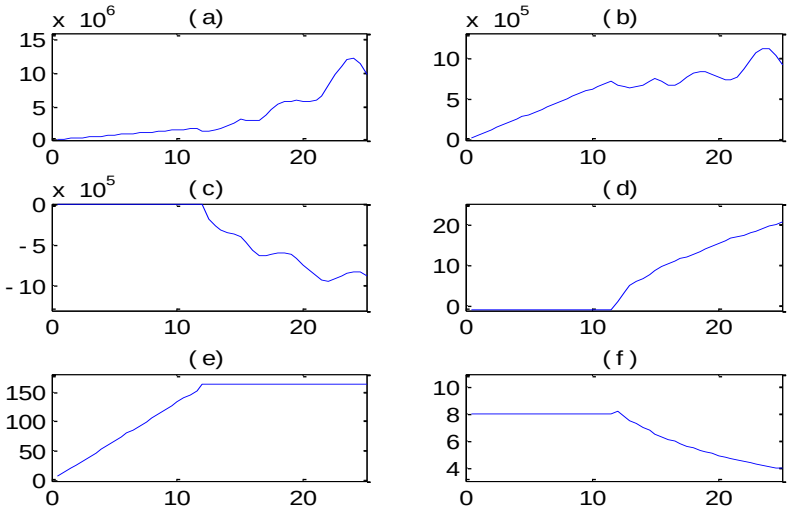

Fig 5 Parameters along the normal operating trajectory

It can be seen from Fig 5 that it is not easy to find a suitable function to fit these discontinuous relationships. Since gridding methods do not impose restrictions on the parameter dependence of the LPV model, and it is not required to derive mathematical expressions or find polynomial approximations for the gains of T_{r,ω_r}, $T_{r,\beta}$ and $T_{r,v}$. Lookup tables can be used with suitable interpolation to find the corresponding parameters during simulation or real system implementation.

From an FTC point of view, the three different blade pitch actuators may have individual faults. In addition, another variable ω_{gi} representing the integration of ω_g, is introduced to maintain consistency with the baseline controller design for this

integrated AFTC design. Hence, an LPV system is proposed for the AFTC of the wind turbine system as:

$$\dot{x} = Ax + B\begin{bmatrix}\beta_r \\ T_{g,r}\end{bmatrix} + F_a f_a + Rd \tag{18}$$

$$y = Cx + F_s f_s + Dd \tag{19}$$

where:

$$x^T = \begin{bmatrix}\omega_r & \omega_g & \theta_\Delta & \omega_{gi} & T_g & \beta_1 & \dot{\beta}_1 & \beta_2 & \dot{\beta}_2 & \beta_3 & \dot{\beta}_3\end{bmatrix}$$

$$A = \begin{bmatrix}A_{dt0} & \Delta_{10} & \Delta_{20} \\ 0 & A_{g0} & 0 \\ 0 & 0 & A_{ps0}\end{bmatrix}, C = \begin{bmatrix}C_{dt0} & 0 & 0 \\ 0 & C_{g0} & 0 \\ 0 & 0 & C_{ps0}\end{bmatrix}, B = \begin{bmatrix}0 & 0 \\ B_{g0} & 0 \\ 0 & B_{ps0}\end{bmatrix}$$

$$A_{ps} = \begin{bmatrix}A_\beta & 0 & 0 \\ 0 & A_\beta & 0 \\ 0 & 0 & A_\beta\end{bmatrix}, A_\beta = \begin{bmatrix}0 & 1 \\ -\omega_{n0}^2 & -2\varsigma_0\omega_{n0}\end{bmatrix}$$

$$A_{dt} = \begin{bmatrix} a_{11} & \frac{B_{dt}}{N_g J_r} & \frac{-K_{dt}}{J_r} & 0 \\ \frac{\eta_{dt}B_{dt}}{N_g J_g} & a_{22} & \frac{\eta_{dt}K_{dt}}{N_g J_g} & 0 \\ 1 & -\frac{1}{N_g} & 0 & 0 \\ 0 & 1 & 0 & 0 \end{bmatrix}, \Delta_{20} = \begin{bmatrix} \frac{T_{r,\beta}}{3J_r} & 0 & \frac{T_{r,\beta}}{3J_r} & 0 & \frac{T_{r,\beta}}{3J_r} & 0 \\ 0 & 0 & 0 & 0 & 0 & 0 \\ 0 & 0 & 0 & 0 & 0 & 0 \\ 0 & 0 & 0 & 0 & 0 & 0 \end{bmatrix}$$

$$A_{g0} = -50, \Delta_{10} = \frac{T_{r,g}}{J_g}, a_{11} = -\frac{B_{dt} + B_r}{J_r} + \frac{T_{r,\omega_r}}{J_r}, a_{22} = -\frac{\eta_{dt}B_{dt}}{N_g^2 J_g} - \frac{B_g}{J_g}$$

$$B_{dt0} = \begin{bmatrix}\frac{T_{r,v}}{J_r} & 0 & 0 & 0 & 0\end{bmatrix}^T, B_{g0} = -\frac{1}{J_g}, B_{ps0} = \begin{bmatrix}\omega_{n0}^2 & 0 & 0 & 0 & 0 \\ 0 & 0 & \omega_{n0}^2 & 0 & 0 \\ 0 & 0 & 0 & 0 & \omega_{n0}^2\end{bmatrix}^T$$

$$C_{g0} = 1, C_{dt0} = \begin{bmatrix}1 & 0 & 0 & 0 \\ 1 & 0 & 0 & 0 \\ 0 & 1 & 0 & 0 \\ 0 & 1 & 0 & 0 \\ 0 & 0 & 0 & 1\end{bmatrix}, C_{ps0} = \begin{bmatrix}1 & 0 & 0 & 0 & 0 & 0 \\ 1 & 0 & 0 & 0 & 0 & 0 \\ 0 & 0 & 1 & 0 & 0 & 0 \\ 0 & 0 & 1 & 0 & 0 & 0 \\ 0 & 0 & 0 & 0 & 1 & 0 \\ 0 & 0 & 0 & 0 & 1 & 0\end{bmatrix}$$

$$F_a = \begin{bmatrix} 0 & 0 & 0 & 0 & 0 & -\frac{1}{J_g} & 0 & 0 & 0 & 0 & 0 \\ 0 & 0 & 0 & 0 & 0 & 0 & 1 & 0 & 0 & 0 & 0 \\ 0 & 0 & 0 & 0 & 0 & 0 & 0 & 0 & 1 & 0 & 0 \end{bmatrix}^T, R = \begin{bmatrix} B_{dt0} & 0 \\ 0 & 0 \\ 0 & 0 \end{bmatrix}$$

$$F_s = \begin{bmatrix} 1 & 0 & 0 & 0 & 0 & 0 & 0 & 0 & 0 & 0 & 0 & 0 \\ 0 & 0 & 1 & 0 & 0 & 0 & 0 & 0 & 0 & 0 & 0 & 0 \\ 0 & 0 & 0 & 0 & 0 & 0 & 0 & 0 & 0 & 1 & 0 & 0 \\ 0 & 0 & 0 & 0 & 0 & 0 & 0 & 0 & 0 & 0 & 1 & 0 \end{bmatrix}^T$$

$$D = \begin{bmatrix} 0.01 & 0.01 & 0 & 0 & 0 & 0 & 0 & 0 & 0 & 0 & 0 & 0 \\ 0 & 0 & .1 & .1 & 0 & 0 & 0 & 0 & 0 & 0 & 0 & 0 \\ 0 & 0 & 0 & 0 & 0 & 90 & 0 & 0 & 0 & 0 & 0 & 0 \\ 0 & 0 & 0 & 0 & 0 & 0 & 0.2 & 0.2 & 0.2 & 0.2 & 0.2 & 0.2 \end{bmatrix}^T$$

3.3 Integrated design of the AFTC system

In this study, the full load region is the main consideration because the pitch angles are held constant at an optimal value in the partial load region. However, in Section 5, it is shown that the schemes developed for the high wind speed region can also work well at low wind speeds.

In the high wind speed region, the parameters of the closed-loop system can be encapsulated by a two-vertices-polytope. With the a defined system state x_a, the wind turbine system can be augmented as:

$$E_a \dot{x}_a = A_a x_a + B_a \begin{bmatrix} \beta_r \\ T_{g,r} \end{bmatrix} + R_a d \tag{20}$$

$$y = C_a x_a + D d \tag{21}$$

where:

$$x_a^T = \begin{bmatrix} \omega_r & \omega_g & \theta_\Delta & \omega_{gi} & f_{rs} & f_{gs} & T_g & f_{tg} & \beta_1 & \dot{\beta}_1 \\ & & & & & & & & f_{\beta 1} & \delta_1 & \beta_2 & \dot{\beta}_2 & f_{\beta 2} & \delta_2 & f_{\beta s2} & \beta_3 & \dot{\beta}_3 & f_{\beta s3} \end{bmatrix}$$

$$E_a = \begin{bmatrix} E_{dt} & 0 & 0 \\ 0 & E_g & 0 \\ 0 & 0 & E_{ps} \end{bmatrix}, A_a = \begin{bmatrix} A_{dt} & \Delta_1 & \Delta_2 \\ 0 & A_g & 0 \\ 0 & 0 & A_{ps} \end{bmatrix}, C_a = \begin{bmatrix} C_{dt} & 0 & 0 \\ 0 & C_g & 0 \\ 0 & 0 & C_{ps} \end{bmatrix}, E_g = I_2$$

$$E_{\beta1} = I_2, E_{\beta2} = \begin{bmatrix} I_2 & 0 \\ 0 & 0 \end{bmatrix}, E_{\beta3} = \begin{bmatrix} I_2 & 0 \\ 0 & 0 \end{bmatrix}, E_{ps} = \begin{bmatrix} E_{\beta1} & 0 & 0 \\ 0 & E_{\beta2} & 0 \\ 0 & 0 & E_{\beta3} \end{bmatrix}, E_{dt} = \begin{bmatrix} I & 0 & 0 \\ 0 & 0 & 0 \\ 0 & 0 & 0 \end{bmatrix}$$

$$A_{\beta1} = \begin{bmatrix} A_\beta & F_\beta & 0 \\ 0 & 0 & 1 \\ 0 & 0 & 0 \end{bmatrix}, A_{\beta2} = \begin{bmatrix} A_{\beta1} & 0 \\ 0 & 0 \end{bmatrix}, A_{\beta3} = \begin{bmatrix} A_\beta & 0 \\ 0 & 0 \end{bmatrix}, A_{ps} = \begin{bmatrix} A_{\beta1} & 0 & 0 \\ 0 & A_{\beta2} & 0 \\ 0 & 0 & A_{\beta3} \end{bmatrix}$$

$$A_g = \begin{bmatrix} -50 & -50 \\ 0 & 0 \end{bmatrix}, A_{dt} = \begin{bmatrix} A_{dt0} & 0 & 0 \\ 0 & 0 & 0 \\ 0 & 0 & 0 \end{bmatrix}, B_a = \begin{bmatrix} B_{dt} & 0 & 0 \\ 0 & B_g & 0 \\ 0 & 0 & B_{ps} \end{bmatrix}$$

$$\Delta_{20} = \begin{bmatrix} \frac{T_{r,\beta}}{3J_r} & 0 & 0 & 0 & \frac{T_{r,\beta}}{3J_r} & 0 & 0 & 0 & 0 & \frac{T_{r,\beta}}{3J_r} & 0 & 0 \\ 0 & 0 & 0 & 0 & 0 & 0 & 0 & 0 & 0 & 0 & 0 & 0 \\ 0 & 0 & 0 & 0 & 0 & 0 & 0 & 0 & 0 & 0 & 0 & 0 \\ 0 & 0 & 0 & 0 & 0 & 0 & 0 & 0 & 0 & 0 & 0 & 0 \\ 0 & 0 & 0 & 0 & 0 & 0 & 0 & 0 & 0 & 0 & 0 & 0 \\ 0 & 0 & 0 & 0 & 0 & 0 & 0 & 0 & 0 & 0 & 0 & 0 \end{bmatrix}, \Delta_1 = \begin{bmatrix} \frac{T_{r,g}}{J_g} & 0 \end{bmatrix},$$

$$B_{dt} = \begin{bmatrix} \frac{T_{r,v}}{J_r} & 0 & 0 & 0 & 0 & 0 \end{bmatrix}^T, B_g = \begin{bmatrix} -\frac{1}{J_g} & 0 \end{bmatrix}$$

$$B_{ps} = \begin{bmatrix} \omega_{n0}^2 & 0 & 0 & 0 & 0 & 0 & 0 & 0 & 0 & 0 & 0 & 0 \\ 0 & 0 & 0 & 0 & 0 & 0 & 0 & 0 & 0 & 0 & 0 & 0 \\ 0 & 0 & 0 & 0 & \omega_{n0}^2 & 0 & 0 & 0 & 0 & 0 & 0 & 0 \\ 0 & 0 & 0 & 0 & 0 & 0 & 0 & 0 & 0 & \omega_{n0}^2 & 0 & 0 \end{bmatrix}^T, C_g = [1 \quad 0]$$

$$C_{dt} = \begin{bmatrix} 1 & 0 & 0 & 0 & 1 & 0 \\ 1 & 0 & 0 & 0 & 0 & 0 \\ 0 & 1 & 0 & 0 & 0 & 1 \\ 0 & 1 & 0 & 0 & 0 & 0 \\ 0 & 0 & 0 & 1 & 0 & 0 \end{bmatrix}, C_{ps} = \begin{bmatrix} 1 & 0 & 0 & 0 & 0 & 0 & 0 & 0 & 0 & 0 & 0 & 0 \\ 1 & 0 & 0 & 0 & 0 & 0 & 0 & 0 & 0 & 0 & 0 & 0 \\ 0 & 0 & 0 & 0 & 1 & 0 & 0 & 0 & 0 & 0 & 0 & 0 \\ 0 & 0 & 0 & 0 & 1 & 0 & 0 & 0 & 1 & 0 & 0 & 0 \\ 0 & 0 & 0 & 0 & 0 & 0 & 0 & 0 & 0 & 1 & 0 & 1 \\ 0 & 0 & 0 & 0 & 0 & 0 & 0 & 0 & 0 & 1 & 0 & 0 \end{bmatrix}$$

$$D = \begin{bmatrix} 0.01 & 0.01 & 0 & 0 & 0 & 0 & 0 & 0 & 0 & 0 & 0 & 0 \\ 0 & 0 & 0.1 & 0.1 & 0 & 0 & 0 & 0 & 0 & 0 & 0 & 0 \\ 0 & 0 & 0 & 0 & 0 & 90 & 0 & 0 & 0 & 0 & 0 & 0 \\ 0 & 0 & 0 & 0 & 0 & 0 & 0.2 & 0.2 & 0.2 & 0.2 & 0.2 & 0.2 \end{bmatrix}^T$$

A descriptor LPV ESO is designed for the descriptor system of (21) and (22), in the following form:

$$E_a \dot{\hat{x}}_a = A_a(\theta)\hat{x}_a + B_a \begin{bmatrix} \beta_r \\ T_{g,r} \end{bmatrix} + L(\theta)(\hat{y} - y) \tag{22}$$

$$\hat{y} = C_a \hat{x}_a \tag{23}$$

The control strategy proposed in (15) is considered with the baseline controller presented in Section 2.5. With the closed-loop system states constructed with original states and estimation errors, the following closed-loop system is obtained:

$$E_{cl} \begin{bmatrix} \dot{x} \\ \dot{e}_{xf} \end{bmatrix} = A_{cl} \begin{bmatrix} x \\ e_{xf} \end{bmatrix} + R_{cl} d \tag{24}$$

where:

$$E_{cl} = \begin{bmatrix} I & 0 \\ 0 & E_a \end{bmatrix}, A_{cl} = \begin{bmatrix} A(\theta) + BKC & \Delta \\ 0 & A_o(\theta) \end{bmatrix}$$

$$\Delta = [BKC \quad 0 \quad F_a], R_{cl} = \begin{bmatrix} R \\ R_a + L(\theta)D \end{bmatrix}, A_o(\theta) = A_a(\theta) + L(\theta)C$$

where K corresponds to the baseline controller designed in Section 3, and L is the ESO gain to be determined.

Define the H_∞ performance variable as:

$$z_{xef} = C_z \begin{bmatrix} \dot{x} \\ \dot{e}_{xf} \end{bmatrix} \tag{25}$$

where $C_z = [C_{zx} \quad C_{zexf}]$ is a weighting matrix. Then the transfer function from disturbance or modelling uncertainty d to the performance variable z_{xef} can be obtained as:

$$G_{cl}(\theta, s) = C_z (sE_{cl} - A_{cl})^{-1} R_{cl}$$

Based on the Bound Real Lemma of LPV descriptor systems proposed in [20], the closed-loop system of (24) and (25) is admissible and $\|G_{cl}(\theta, s)\|_\infty < \gamma$ if there exist $\mathcal{P} > 0, \mathcal{S}$ with compatible dimensions selected as:

$$\mathcal{P} = \begin{bmatrix} P & 0 \\ 0 & Q \end{bmatrix}, \mathcal{S} = \begin{bmatrix} S & 0 \\ 0 & W \end{bmatrix}$$

such that:

$$\begin{bmatrix} \Delta_{11} & \Delta_{12} & (E^T P + USV^T)R & C_{zx}^T \\ \star & \Delta_{22} & \Delta_{23} & C_{ze}^T \\ \star & \star & -\gamma & 0 \\ \star & \star & \star & -\gamma \end{bmatrix} < 0 \tag{26}$$

with:

$$\Delta_{11}(\theta) = (E^T P + USV^T)(A(\theta) + BKC) + \star$$

$$\Delta_{12}(\theta) = (E_a^T Q + U_a W V_a^T)[BK(\theta)C \quad 0 \quad F_{ag} \quad F_{aps}]$$

$$\Delta_{22}(\theta) = (E_a^T Q + U_a W V_a^T)(A_a(\theta) + LC_a) + \star$$

$$\Delta_{23} = (E_a^T Q + U_a W V_a^T)(R_a + LD)$$

where U_a and V_a are full column rank and contain the basis vectors for $Ker(E_a)$ and $Ker(E_a^T)$, U and V are full column rank and contain the basis vectors for $Ker(E)$ and $Ker(E^T)$, respectively.

Furthermore, it is proposed to use a parameter independent ESO gain with a special structure as follows:

$$L = \begin{bmatrix} L_{dt} & 0 & 0 \\ 0 & L_g & 0 \\ 0 & 0 & L_{ps} \end{bmatrix}$$

where L_{dt} ,L_g ,L_{ps} are to be determined. One benefit arising from using the diagonal structure is that the problem of pole-placement of the subsystems into separate LMI regions can be simplified, as shown in the following. With the constant observer gain L, the observer system matrix would be:

$$A_o = \begin{bmatrix} A_{dt} + L_{dt}C_{dt} & \Delta_1 & \Delta_2 \\ 0 & A_g + L_gC_g & 0 \\ 0 & 0 & A_{ps} + L_{ps}C_{ps} \end{bmatrix}$$

Furthermore:

$$E_{cl} = \begin{bmatrix} I & 0 \\ 0 & E_a \end{bmatrix}, E_a = \begin{bmatrix} E_{dt} & 0 & 0 \\ 0 & E_g & 0 \\ 0 & 0 & E_{ps} \end{bmatrix}$$

which means that the null space of E_{cl} can be specified in terms of E_a as follows:

$$U_{cl} = \begin{bmatrix} 0 \\ U_a \end{bmatrix}, V_{cl} = \begin{bmatrix} 0 \\ V_a \end{bmatrix}, U_a = \begin{bmatrix} U_{dt} & 0 & 0 \\ 0 & U_g & 0 \\ 0 & 0 & U_{ps} \end{bmatrix}, V_a = \begin{bmatrix} V_{dt} & 0 & 0 \\ 0 & V_g & 0 \\ 0 & 0 & V_{ps} \end{bmatrix}$$

where U_{dt} and V_{dt} are full column rank and contain the basis vectors for $Ker(E_{dt})$ and $Ker(E_{dt}^T)$, respectively. $U_g$and V_g are full column rank and contain the basis vectors for $Ker(E_g)$ and $Ker(E_g^T)$, respectively. U_{ps} and V_{ps} are full column rank and contain the basis vectors for $Ker(E_{ps})$ and $Ker(E_{ps}^T)$, respectively. Furthermore, the structure of $Q$and W are specified as:

$$Q = \begin{bmatrix} Q_{dt} & 0 & 0 \\ 0 & Q_g & 0 \\ 0 & 0 & Q_{ps} \end{bmatrix}, W = \begin{bmatrix} W_1 & 0 & 0 \\ 0 & W_2 & 0 \\ 0 & 0 & W_3 \end{bmatrix}$$

Following the procedure proposed in [20], set:

$$Y_{dt} = Q_{dt}L_{dt}, Y_g = Q_gL_g, Y_{ps} = Q_{ps}L_{ps}$$

$$H_1 = W_1U_{a1}^TL_{dt}, H_2 = W_2U_{a2}^TL_g, H_3 = W_3U_{a3}^TL_{ps}$$

Then $\Delta_{22}(\theta)$can be partitioned as:

$$\Delta_{22}(\theta) = \Delta_{22a} + \Delta_{22b}$$

with:

$$\Delta_{22a}=\begin{bmatrix} E_{dt}^T Q_{dt} A_{dt} + E_{dt}^T Y_{dt} C_{dt} & E_{dt}^T Q_{dt} \Delta_1 & E_{dt}^T Q_{dt} \Delta_2 \\ 0 & Q_g A_g + Y_g C_g & Q_g \Delta_3 \\ 0 & 0 & Q_{ps} A_{ps} + Q_{ps} C_{ps} \end{bmatrix} + \star$$

$$\Delta_{22b}=\begin{bmatrix} U_{dt} W_1 V_{dt}^T A_{dt} + U_{dt} H_1 C_{dt} & U_{dt} W_1 V_{dt}^T \Delta_1 & U_{dt} W_1 V_{dt}^T \Delta_2 \\ 0 & U_g W_2 V_g^T A_g + U_g H_2 C_g & U_g W_2 V_g^T \Delta_3 \\ 0 & 0 & F_{1b33} \end{bmatrix} + \star$$

$$\Delta_{22b33}= U_{ps} W_3 V_{ps}^T A_{ps} + U_{ps} H_3 C_{ps}$$

Furthermore, from the structure of $\Delta_{22}(\theta)$, it can be observed that the eigenvalues of one subsystem will not affect that of another subsystem. Based on the pole-placement techniques for LPV descriptor system discussed in [20], the eigenvalues of each subsystem can be assigned into corresponding desired regions. Similarly, the LMIs can be obtained to constrain the subsystem poles in different regions. For example, the generator and converter subsystem must respond in a faster time-scale than the drive train subsystem, so that the relative magnitudes of the corresponding eigenvalues should be assigned to reflect this physical feature.

Then, the problem is solved using MATLAB LMITOOL box. The observer gain obtained is:

$$L_{dt1} = \begin{bmatrix} 0.079127 & -0.27673 & 3.2339 & -39.821 & 89.929 \\ 1.1142 & -4.6811 & 19.971 & -436.07 & 866.55 \\ 0.00053798 & -0.0029312 & 0.00064773 & -0.61229 & 1.5252 \\ 0.30049 & -1.5161 & -5.2508 & -53.497 & 77.101 \\ -64.93 & 64.93 & -7.38\text{e}-6 & 4.54\text{e}-5 & -9\text{e}-5 \\ -1.54\text{e}-5 & 4.46\text{e}-5 & -64.934 & 64.926 & 0.02154 \end{bmatrix}$$

$$L_g = \begin{bmatrix} -41.339 \\ -41.339 \end{bmatrix}$$

$$L_{ps} = \begin{bmatrix} -3.2697 & -15.174 & -0.62933 & 0.053112 & 2.423 & 13.213 \\ -1.3461 & -6.8059 & -10.509 & 0.21928 & -5.2258 & 54.122 \\ -2.5241 & -15.029 & -0.58687 & 0.094432 & 2.4302 & 15.616 \\ -8.7472 & 9.234 & -0.19209 & -0.067579 & -0.036529 & -0.19056 \\ 3.1015 & 4.9546 & -28.066 & -9.5366 & 5.6402 & 20.522 \\ 43.478 & 67.415 & -215.42 & -96.509 & 46.656 & 184.84 \\ 8.5534 & 14.193 & -55.379 & -21.485 & 12.928 & 41.189 \\ 35.228 & 59.995 & -175.27 & -81.372 & 46.132 & 115.29 \\ -0.0531 & -0.20429 & 9.4546 & -8.7183 & -0.081393 & -0.39747 \\ 0.19163 & 0.67649 & 0.16837 & 0.00071 & -0.98538 & -3.4362 \\ 1.3319 & -5.2952 & -9.5992 & -0.19567 & -7.4994 & 51.712 \\ -0.0517 & -0.17886 & -0.40926 & -0.066921 & -8.7343 & 9.441 \end{bmatrix}$$

4 Simulation results

The simulations are carried out within the MATLAB/SIMULINK environment. The results are presented separately in the Subsection 5.1. The simulations are carried out based on the wind speed time signal shown in Fig 6 using the principle proposed in [1].

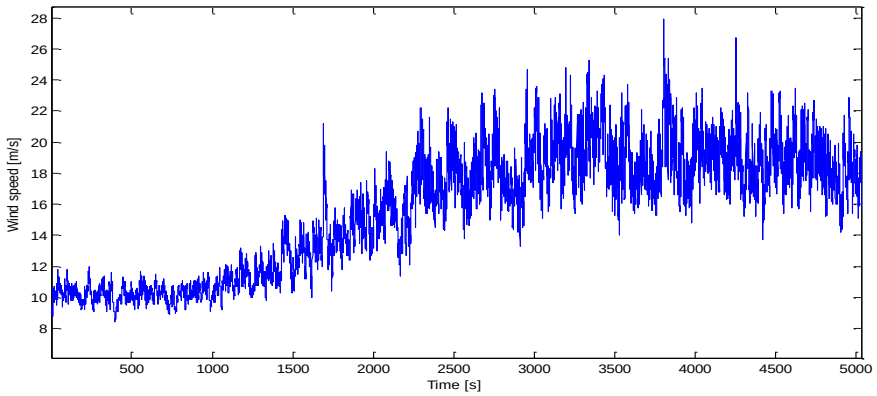

Fig 6 Wind speed used for evaluation

One important feature of the wind speed is that the magnitude of the disturbance becomes larger when the wind speed increases, which is due to the nature of the wind turbulence.

4.1 Faults in pitch subsystems

The results arising from the pitch subsystem fault scenarios are presented in terms of pitch angle variations with their estimates and measured outputs (using pitch angle

sensors) in Figs 7, 8 & 9. It is easy to know whether or not a fault has occurred from the provided estimation results. For instance in Fig 7, it is clear that a pitch sensor fault occurred during 2000s-2100 since the measurement is far away from the estimate of pitch angle. The estimation of the fault signal f_β re-defined according to (11), is shown in Fig 10. With the estimated actuator fault signal, AFTC is carried out with the strategy presented in Section 4. The AFTC results are shown in Figs 11 & 12.

To show the improvement of the AFTC scheme in the simulation, one criteria function is defined as:

$$\gamma_\beta = \frac{\sum_{i=1}^{n_\beta} e_{FTC\beta i}}{\sum_{i=1}^{n_\beta} e_{\beta i}}$$

where n_β is the number of samples during the simulation, $e_{FTC\beta i}$ is the error of the faulty pitch angle from the fault-free angle with FTC activated, $e_{\beta i}$ is the error of the faulty pitch angle from the fault-free pitch angle without FTC activated. Therefore, $\gamma_\beta < 1$ means there is improvement of AFTC. In the simulation, the γ_β is obtained as $\gamma_\beta = 0.8172$. Hence, the performance of the wind turbine system is improved by the AFTC when there is a pitch actuator fault.

One problem arising from re-defining the fault signal is that it is not easy to decide the severity of a fault as it is strongly coupled to the system states. The real fault signal can be constructed using the approach proposed in Section 2.4. The reconstructed fault is shown in the Fig 13 from which it is very easy to determine whether there is a fault or not and also the severity of the fault. The result given in Fig 13 corresponds to the case of oil with abnormally high air content – with expected fault severity of θ_f =1.

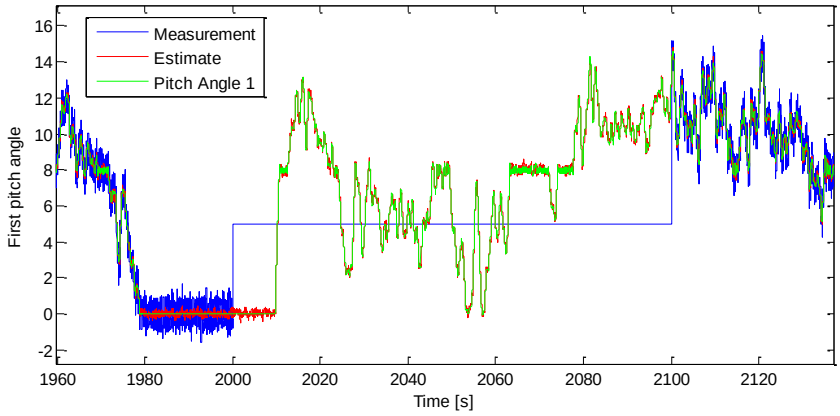

Fig 7 First pitch angle state, measurement and estimate with sensor fault

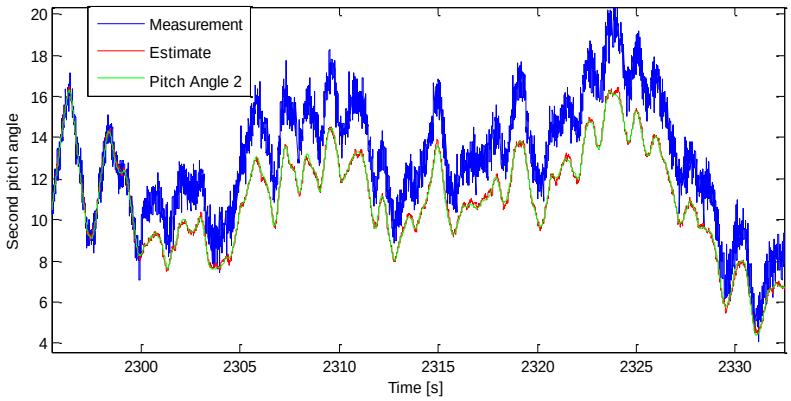

Fig 8 Second pitch angle state, measurement and estimate with sensor fault

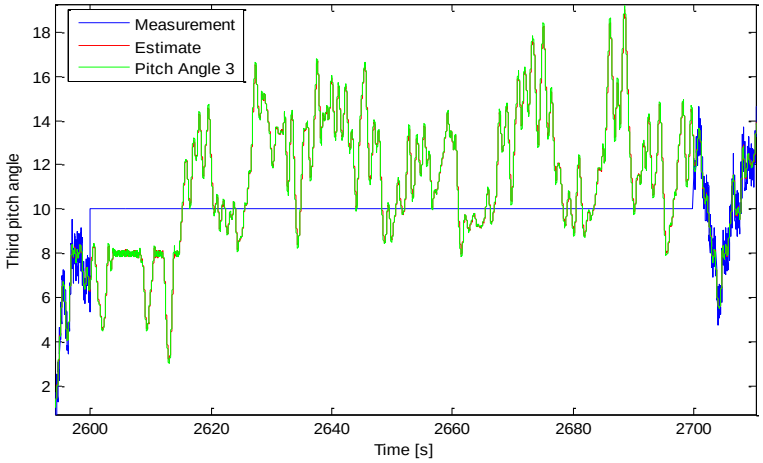

Fig 9 Third pitch angle state, measurement and estimate with sensor fault

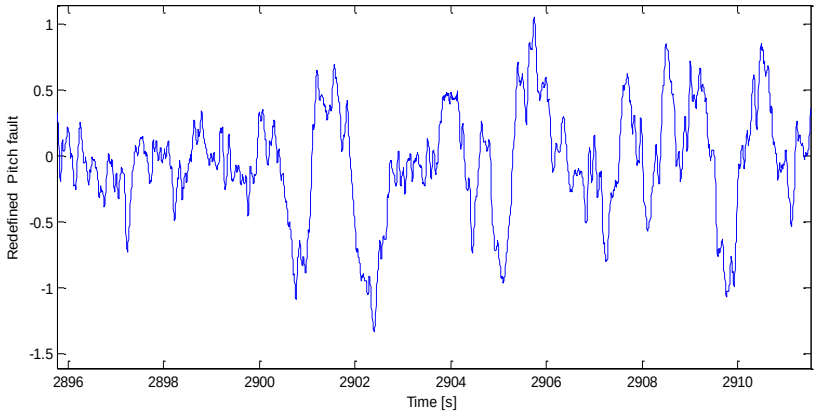

Fig 10 Estimate of the newly defined fault f_β

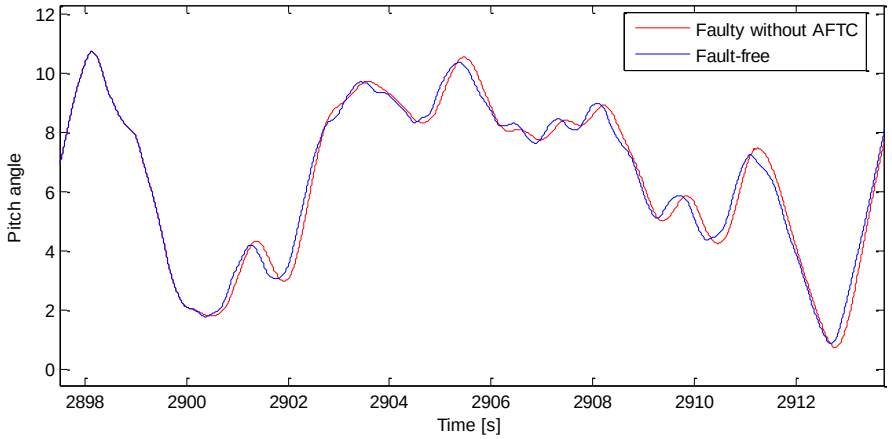

Fig 11 Pitch angles with fault occurring without AFTC

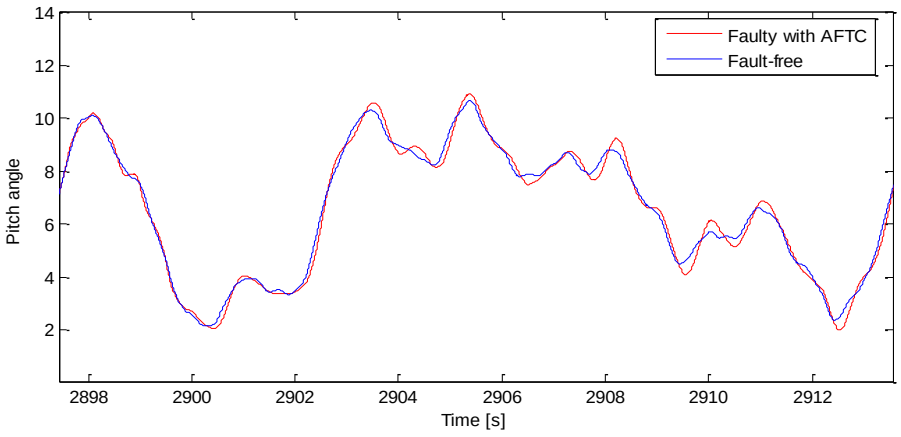

Fig 12 Pitch angles with AFTC activated

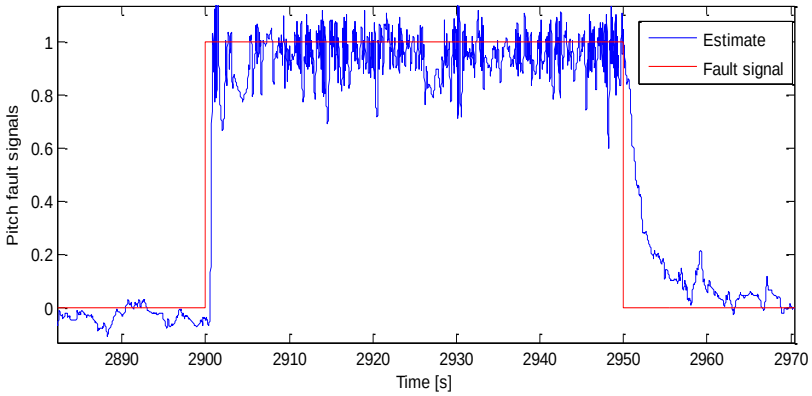

Fig 13 Fault θ_f and its estimate in the high air content case

4.2 Actuator fault in generator subsystem

The estimation of the torque actuator fault is presented in Fig 14 (a). It can be seen that the LPV ESO method can provide very good fault estimation, which is a significant result even though it is claimed that a 100 Nm fault is too small to be detected [13].From the simulation results, there is no obvious improvement obtained by using the AFTC scheme. However, generator torque offsets will result in large amount of lost energy production over time. In addition, tt is important to point out that the actuator fault should be detected as early as possible to prevent the impact of faults from other subsystems, or even to prevent a gross effect on the overall system performance. To test the robustness of the fault estimation at different operation points, another scenario that the fault occurred between 3100s-3200s is carried out and the simulation result is given in Fig 14 (b).

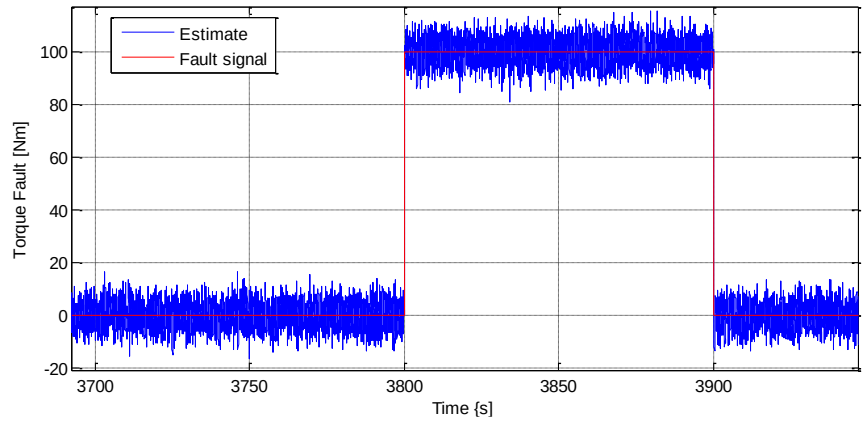

(a)

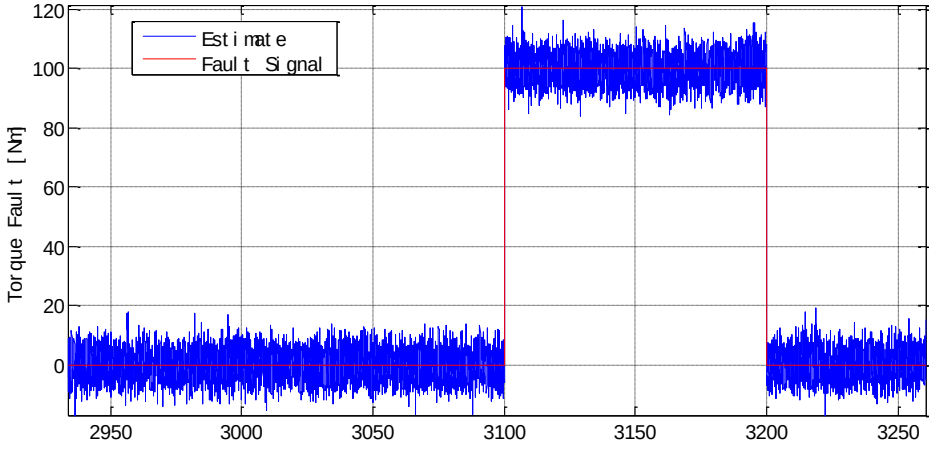

(b)

Fig 14 Generator torque fault and estimate

4.3 Generator speed sensor fault

The generator speed is simulated with a constant bias fault during 1000s-1100s. The simulation results are shown in Fig 15 where it can be seen that the rotor speed estimation follows the real rotor speed closely whether or not a fault has occurred.

For the result shown in Fig 16, the AFTC uses sensor hiding. The output power P_g response is shown (calculated from (5)) with and without the AFTC switched on and corresponding to different output conditions. It is clear that the quality of the output power is improved as the smoothness is an important property considering that the

converter can be damaged by the large transient shown (in the red curve) by the keeping the AFTC system switched off.

The estimated rotor speed shown in Fig 17 shows that for the fault-free case, the estimate is closer to the real signal compared with the measurement disturbed by sensor noise. The rotor speed stuck-value sensor fault is simulated during 1500s-1600s. The estimate tracks the real signal closely even after the fault has occurred. As the rotor speed is not involved in the feedback control loop, the rotor speed sensor fault will not affect the closed-loop system performance.

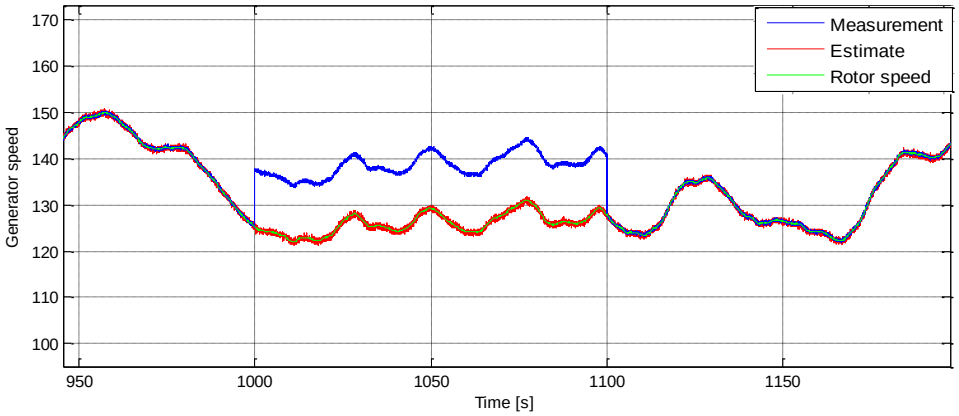

Fig 15 Generator speed state, measurement and estimate with sensor fault

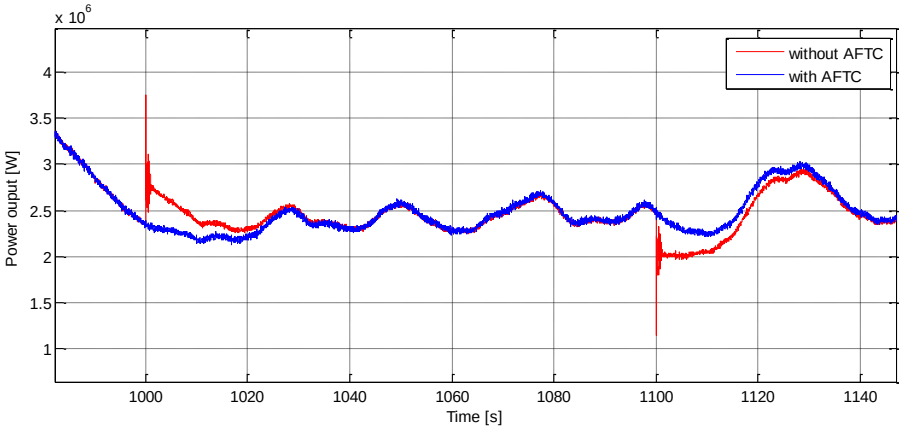

Fig 16 Power output with and without AFTC activated

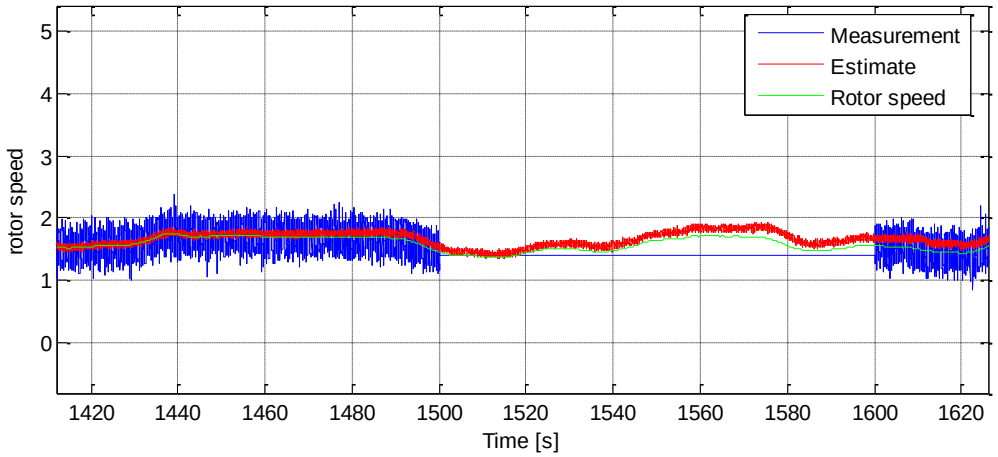

Fig 17 Rotor speed state, measurement and estimate

5 Conclusion

An observer-based descriptor system AFTC scheme is designed for an offshore wind turbine system using a robust LPV framework to account for modelling uncertainty arising from (a) parameter variations in the system, (b) uncertain knowledge of the effective wind speed, and (c) sensor noise. Both the faults and the required baseline controller system states are estimated using the proposed descriptor system LPV ESO formulated within an LPV framework. The AFTC uses an output feedback baseline controller corresponding to a typically implemented controller. It is shown that the AFTC design is capable of stabilizing both the faulty and fault-free systems. The use of a typical control system within the baseline controller structure means that the system can easily be viewed as an extension of currently used control technology, with the AFTC proving clear "added value" as a fault tolerant system, to enhance the sustainability of the wind turbine in the offshore environment.

References

1. Burton, T., Sharpe, D., Jenkins, N. and Bossanyi, E., *Wind energy handbook*2001, Chichester: John Wiley & Sons Ltd.
2. Gsänger, S. and Pitteloud, J.-D., *World Wind Energy Report 2012*, 2013, World Wind Energy Association WWEA: Bonn,Germany.
3. Pao, L.Y. and Johnson, K.E., *Control of wind turbines.* IEEE Control Systems, 2011. **31**(2): p. 44-62.

4. Laks, J.H., Pao, L.Y. and Wright, A.D. *Control of wind turbines: past, present, and future*. in *American Control Conference*. 2009.
5. Bianchi, F.D., Battista, H.D. and Mantz, R.J., *Wind turbine control systems: principles,modelling and gain scheduling design*. Advances in Industrial Control, ed. M.J. Grimble and M.A. Johnson2007, Germany: Springer-Verlag London Limited.
6. Esbensen, T. and Sloth, C., *Fault diagnosis and fault-tolerant control of wind turbines*, in *Faculty of Engineering, Science and Medicine Department of Electronic Systems Section for Automation and Control*2009, Aalborg Univeristy: Fredrik Bajers, Denmark. p. 167.
7. Boukhezzar, B., Lupu, L., Siguerdidjane, H. and Hand, M., *Multivariable control strategy for variable speed, variable pitch wind turbines.* Renewable Energy, 2007. **32**(8): p. 1273-1287.
8. Leithead, W.E., de la Salle, S. and Reardon, D., *Role and objectives of control for wind turbines.* IEE Proceedings C (Generation, Transmission and Distribution), 1991. **138**(2): p. 135-148.
9. Leithead, W.E. and Connor, B., *Control of variable speed wind turbines: Design task.* International Journal of Control, 2000. **73**(13): p. 1189-1212.
10. Bossanyi, E., Savini, B., Iribas, M., et al., *Advanced controller research for multi - MW wind turbines in the UPWIND project.* Wind Energy, 2012. **15**(1): p. 119-145.
11. Odgaard, P.F. and Johnson, K.E. *Wind turbine fault detection and fault tolerant control - An enhanced benchmark challenge*. in *American Control Conference (ACC), 2013*. 2013.
12. Odgaard, P.F., Stoustrup, J. and Kinnaert, M. *Fault Tolerant Control of Wind Turbines – a benchmark model*. in *7th IFAC Symposium on Fault Detection, Supervision and Safety of Technical Processes*. 2009. Barcelona, Spain.
13. Odgaard, P.F. and Stoustrup, J. *Results of a wind turbine fdi competition*. in *Proceedings of Safeprocess*. 2012.
14. Kamal, E. and Aitouche, A., *Robust fault tolerant control of DFIG wind energy systems with unknown inputs.* Renewable Energy, 2013. **56**(0): p. 2-15.
15. Simani, S. and Castaldi, P., *Active actuator fault-tolerant control of a wind turbine benchmark model.* International Journal of Robust and Nonlinear Control, 2013.
16. Gálvez-Carrillo, M. and Kinnaert, M., *Sensor fault detection and isolation in doubly-fed induction generators accounting for parameter variations*. Renewable Energy, 2011. **36**(5): p. 1447-1457.
17. Sami, M. and Patton, R.J. *Wind turbine sensor fault tolerant control via a multiple-model approach*. in *UKACC International Conference on Control (CONTROL)*. 2012. IEEE.
18. Masubuchi, I., Akiyama, T. and Saeki, M. *Synthesis of output feedback gain-scheduling controllers based on descriptor LPV system representation*. in *42nd IEEE Conference on Decision and Control*. 2003.
19. Sloth, C., Esbensen, T. and Stoustrup, J., *Robust and fault-tolerant linear parameter-varying control of wind turbines.* Mechatronics, 2011. **21**(4): p. 645-659.
20. Shi, F., *Observer based active fault tolerant control of descriptor systems*, in *school of Engineering*2013, University of Hull: Kingston upon Hull, UK.
21. Hamdi, H., Rodrigues, M., Mechmeche, C., Theilliol, D., and Benhadj Braiek, N. *State estimation for polytopic LPV descriptor systems: application to fault diagnosis*. in *7th IFAC Symposium on Fault Detection, Supervision and Safety of Technical Processes*. 2009. Barcelona, Spain.
22. Anonymous. *The Inside of a Wind Turbine*. 2013 17th January [cited 2013 1st August]; Available from: http://www1.eere.energy.gov/wind/inside_a_wind_turbine.html.